



Impacts of land use and land cover changes on local meteorology and PM_{2.5} concentrations in Changchun, Northeast China

Jiaxin Qiu ^{a,b}, Chunsheng Fang ^{a,b,c}, Naixu Tian ^{d,e}, Haofan Wang ^f, Ju Wang ^{a,b,c,*}

^a College of New Energy and Environment, Jilin University, Changchun 130012, China

^b Key Laboratory of Groundwater Resources and Environment, Ministry of Education, Jilin University, Changchun 130021, China

^c Jilin Province Key Laboratory of Water Resources and Environment, Jilin University, Changchun 130021, China

^d School of Environment, Northeast Normal University, Changchun 130117, China

^e State Environmental Protection Key Laboratory of Wetland Ecology and Vegetation Restoration, School of Environment, Northeast Normal University, Changchun 130117, China

^f School of Atmospheric Sciences, Sun Yat-sen University, Zhuhai 519082, China

ARTICLE INFO

Keywords:

WRF-CMAQ
LULC changes
Local meteorology
PM_{2.5}
Changchun

ABSTRACT

Land use and land cover (LULC) changes have a considerable influence on the surface energy balance, altering regional meteorology and air quality. However, this impact is not quantified in Changchun, an important city in the old industrial base of Northeast China. In this study, based on the Weather Research and Forecasting-Community Multiscale Air Quality (WRF-CMAQ) model, the LULC2017 (LULC data in 2017) and LULC2001 (LULC data in 2001) scenarios were simulated for January and July 2017, respectively, to assess the impact of LULC changes on meteorology and fine particulate matter (PM_{2.5}) concentrations in Changchun. The results show that the sensible heat flux in the urban expansion area (UEA) increased during the daytime, reaching a maximum value of 154 W/m² and 162 W/m², respectively, while the latent heat flux decreased during the daytime, reaching a maximum value of 22.84 W/m² and 180.75 W/m², respectively. Consequently, 2 m temperature (T2) increased by 4 °C and 3 °C, respectively; 10 m wind speed (WS10) increased by 1.05 m/s and 1.60 m/s, respectively; and planetary boundary layer height (PBLH) increased by 100 m and 117 m, respectively. These variations in meteorological factors can substantially impact the spatial distribution of air pollutants. In the UEA, PM_{2.5} concentrations decreased by 34 µg/m³ and 20 µg/m³ in January and July, respectively. The change in SO₄²⁻ accounted for approximately 25% of the total concentration change of PM_{2.5}, with a decrease of approximately 5–6 µg/m³ during the nighttime in January. Secondary organic aerosol (SOA) formed from biogenic volatile organic compounds (BVOC) precursors (BSOA) slightly decreased owing to the reduction in croplands dominated by green vegetation. Meanwhile, PM_{2.5} concentrations in the surrounding areas of the UEA increased significantly in January. The results of the process analysis based on the CMAQ model indicate that the main reason for the spatial variation of PM_{2.5} concentrations is the enhancement of transport and diffusion in the horizontal and vertical directions in the UEA. In January, the negative contribution of vertical advection (ZADV) and horizontal advection (HADV) processes to PM_{2.5} in the UEA increased by 25 µg/m³ and 40 µg/m³, respectively. Vertical diffusion (VDIF) process caused an increase in PM_{2.5} diffusion by 40 µg/m³ and 16 µg/m³ during the daytime and nighttime in the UEA, respectively. In July, the negative contribution of VDIF and HADV processes to PM_{2.5} increased by 40 µg/m³ and 32 µg/m³ during the nighttime in the UEA, respectively.

1. Introduction

In recent years, with rapid economic development and urban expansion, environmental problems such as urban heat island, flooding, and air pollution caused by urbanization have become a public concern

(Civerolo et al., 2007; Zhang et al., 2010). Urbanization has led to significant land use and land cover (LULC) changes, which typically result in reduced surface albedo, increased roughness and thermal inertia (Lu et al., 2023; Wang et al., 2022a). These changes can significantly affect the surface energy balance and further influence regional meteorology,

* Corresponding author at: College of New Energy and Environment, Jilin University, Changchun 130012, China.

E-mail address: wangju@jlu.edu.cn (J. Wang).

which in turn affects the diffusion of pollutants and has a profound impact on air quality (Wang et al., 2022b; Wu et al., 2020; Yang et al., 2021a).

With the development of numerical simulation, scholars usually couple urban canopy models with weather research and forecasting models and air quality models to study the effects of urbanization on regional meteorological and atmospheric environment (Wu et al., 2022a; Yang et al., 2020). Tao et al. (2018) conducted a simulation of urban heat island effect using WRF model coupled with urban canopy model (UCM). The study showed that land use/land cover changes resulted in significant warming of the urban surface at night. In addition, it has been suggested that anthropogenic heat contributes significantly to the urban heat island, and Yu et al. (2014) explored that anthropogenic heat emissions increased the temperature in Beijing by about 0.8–1.2 °C using the UCM and LUCY models. Wang et al. (2014) showed that changes in land use changes induced by urbanization in the Pearl River Delta (PRD) increase annual precipitation by about 30%–40%, while decreasing the frequency of light rainfall and increasing the frequency of heavy rainfall in the city. The construction of tall buildings also increases the surface roughness and the dragging force of airflow within the urban canopy, which in turn reduces the surface wind speed. Liao et al. (2014) used WRF-Chem simulations to study that urbanization in the Yangtze River Delta significantly reduces the wind speed by about 0.7–2.6 m/s.

Changes in meteorological conditions and planetary boundary layer structure due to urbanization also have a significant impact on the transport and diffusion of atmospheric pollutants. Zhu et al. (2017) showed that urban expansion could reduce PM₁₀ by 80 µg/m³ (50%) and increase O₃ by 8–12 ppb in July in South China. Chen et al. (2014) found that SO₂ daily average concentration change due to land use changes in the Pearl River Delta region in winter was 2 µg/m³ at maximum, while the concentration change due to anthropogenic emissions was 6 µg/m³, indicating that the impact of land use change on air quality can not be ignored. Similar results were presented by (Li et al., 2016), who found that circulation induced by urbanization had a significant effect on O₃ concentrations in the PRD region, leading to a decrease of 1.3 ppb during the day and an increase of 5.2 ppb at night. Exploring the effects of urbanization on regional meteorology and air quality has become a hot issue in recent years.

Changchun is a central city in Northeast China, and an important old industrial base in the region. It has experienced rapid urbanization in recent years, with notable urban expansion (Wu et al., 2022b). Dong et al. (2020) interpreted the Landsat remote sensing image data of Changchun from different years and discovered that the land use structure of Changchun changed significantly from 2000 to 2019, particularly the construction land, which showed an intensive urban expansion from 34.0 × 10³ ha to 47.5 × 10³ ha. Because of the city's rapid expansion, the land use and land cover types of the city and its surrounding areas have changed dramatically (Peng et al., 2020). Many previous studies have discussed the effects of LULC changes on regional meteorology and air quality in Changchun. Most relevant studies have focused on meteorological processes (Yang et al., 2017, 2022; Chen and Zhang, 2022; Chen et al., 2022; Yang et al., 2021b), and only a few have investigated the relative contribution of LULC changes to air quality in Changchun (Qi et al., 2023). Additionally, these limited studies have usually focused only on the changes in concentration of pollutants at the surface or in the vertical direction (Shi et al., 2022). Therefore, simulation analyses of the chemical components of pollutants and physical and chemical processes associated with pollutant formation, transport, and diffusion should be performed to advance our understanding.

To fill the knowledge gaps, this study combined 2017 LULC data with the Weather Research and Forecasting-Community Multiscale Air Quality Model (WRF-CMAQ) to quantify the effects of land use changes on meteorological conditions and PM_{2.5} concentrations in Changchun City by comparing them with the default 2001 LULC data. In addition, the contribution of physical and chemical processes in PM_{2.5} formation,

transport and diffusion was quantified by the process analysis module of the CMAQ model to distinguish the dominant factors of LULC changes on PM_{2.5} concentrations.

2. Methodology and data

2.1. Model description and configuration

The WRF-CMAQ (WRFv4.1.2 and CMAQv5.4) model was applied to examine the impacts of LULC changes on regional meteorology and air quality in Changchun, Northeast China. The WRF-CMAQ simulations were conducted on triple nested domains, which was consistent with our previous work (Fang et al., 2022), as shown in Fig. 1. The resolution of the triple nested domain was 27 km × 27 km, 9 km × 9 km, and 3 km × 3 km, covering Northeast China, Jilin Province, and Changchun, respectively. The meteorological conditions generated by WRF were used to drive CMAQ to simulate air pollutants.

In the WRF simulations, the vertical grid structure was 36 layers and the model domain was centered at 46.3° N and 126.41° E on a Lambert map projection. The meteorological inputs were generated using the final analysis (FNL) data from the National Center for Environmental Prediction (NCEP) with a 6 h interval and a spatial resolution of 1° × 1°, and the nested outer layer provides the initial and boundary conditions for the inner layer. The shortwave and longwave radiation schemes were Goddard (Chou et al., 2001) and Rapid Radiative Transfer Model (RRTM) (Mlawer et al., 1997), the microphysical scheme was Purdue Lin (Chen and Sun, 2002), the planetary boundary layer and near-surface scheme were MYJ (Janjić, 1994) and Noah land surface model (LSM) (Ek et al., 2003), and the urban canopy model is the single-layer urban canopy model (UCM) (Kusaka and Kimura, 2004), which considers the actual urban morphology and illustrates good simulation performance (Huszar et al., 2021; Stoddart et al., 2021; Wang et al., 2021). In the CMAQ simulations, the vertical grid structure and the central longitude and latitude were consistent with WRF. The AERO6 aerosol module and the CB06 gas-phase chemical mechanism were used in the CMAQ model. A high-resolution anthropogenic emission inventory (MEIC) developed by Tsinghua University was used (<http://meicmodel.org>) (Li et al., 2017; Zheng et al., 2018), which was downscaled by inventory spatial allocation tools version 2.0 (ISATv2.0) (Wang et al., 2023). MEIC has been widely used in model studies and is capable of reproducing the spatiotemporal distribution of pollutant concentrations in most regions of the country (Fan et al., 2021; Ma et al., 2021; Wei et al., 2021). Model of Emissions of Gases and Aerosols from Nature (MEGAN) (Guenther et al., 2006) version 3.2 was used to calculate biogenic emissions. We simulated the meteorological conditions and air quality in January and July 2017 as representative winter and summer months, respectively. Changchun is located in northeastern China and has four distinct seasons, January and July can represent the meteorological conditions in winter and summer in this study. To reduce the effect of initial conditions, the first 5 days were treated as a spin-up period.

2.2. Process analysis

To probe the magnitude change modulated by advection, deposition, and chemical production/loss changes, the process analysis module (PA) in the CMAQ model was activated in simulations. The physical and chemical processes in PA include vertical advection (ZADV), horizontal advection (HADV), horizontal diffusion (HDIF), vertical diffusion (VDIF), primary emission (EMIS), dry deposition (DDEP), cloud processes (CLDS), gas-phase chemistry (CHEM), and aerosol processes (AERO).

2.3. Model experiment design

In this study, we mainly focused on the direct impact of LULC changes on meteorology and the indirect impact on chemistry through

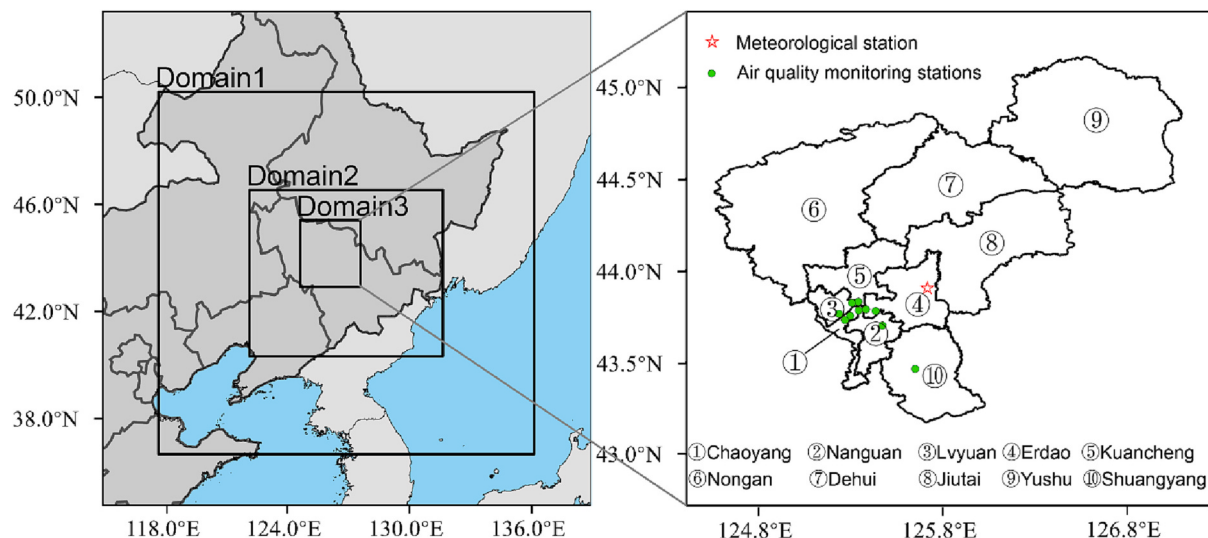


Fig. 1. Map of the triple nested domains for the Weather Research and Forecasting-Community Multiscale Air Quality Model (WRF-CMAQ) model.

physical changes caused by LULC changes. We did not consider the direct effects of LULC changes on chemistry (or anthropogenic emissions). Therefore, the simulation of two land use scenarios was used to investigate the impact of LULC changes in Changchun. LULC2001 scenario represents land use pattern of Changchun and surrounding region in 2001, while LULC2017 scenario depicts land use pattern of Changchun and its surrounding region in 2017. The 2001 LULC data provided by NCAR (National Center for Atmospheric Research) and the 2017 LULC data obtained from the MODIS MCD12Q1. The biogenic emission is not fixed but changes with the LULC changes, and is calculated based on MEGANv3.2 coupled within the CMAQv5.4 model. Except for LULC data, all physical and chemical schemes, as well as anthropogenic emission inventories were identical in both the LULC2017 and LULC2001 scenarios, hence, the difference in the results of the two

simulation scenarios could quantify the impacts of LULC changes on meteorology and air quality in Changchun ([Fig. 2](#), [Table 1](#)).

Table 1
Numerical simulation scenario descriptions.

Scenario definition	LULC	Meteorology data	Anthropogenic emission
LULC2017	2017	FNL_2017	MEIC_2017
LULC2001	2001	FNL_2017	MEIC_2017

LULC, land use and land cover.

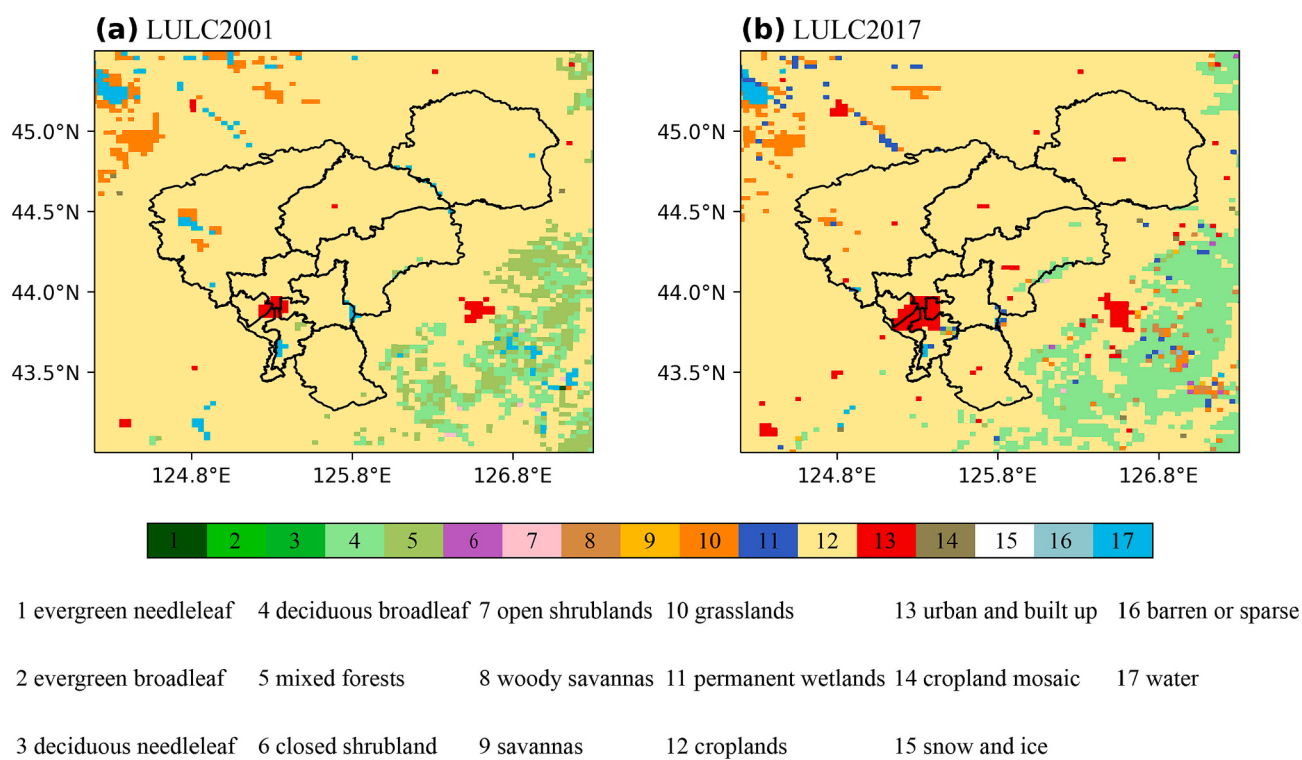


Fig. 2. Land use category for the innermost domain (d03) in LULC2001 (a) and LULC2017 (b). LULC, land use and land cover data.

2.4. The surface observational data

The China Environmental Monitoring Centre (<http://www.cnemc.cn/sssj/>) provided hourly surface observational data of PM_{2.5}. Among the 10 sites in Changchun, nine of them are located in the built-up area of Changchun, namely, the Food Products Factory (FPF), Bus Factory Hospital (BFH), Institute of Posts and Telecommunications (IPT), Labor Park (LP), Garden Management Office (GMO), Jingyue Park (JYP), Economic Development Zone Environment Sanitary Administration (EESA), High-Tech Zone Management Committee (HZMC), Daishan Park (DP), and a clean control site is located in Shuangyang District of Changchun, namely, Shuaiwanzi (SWZ). Due to the close proximity of the monitoring stations, the data from the stations did not differ abruptly from one another and the temporal trends of pollutant concentrations were similar. Therefore, we used one urban station (FPF) and one rural station (SWZ) for model evaluation.

The China Meteorological Data Service Center (<http://data.cma.cn>) also provided hourly ground-level meteorological observations (2 m temperature [T2], 10 m wind speed [WS10]) from national basic meteorological stations (Longjia Airport (LJ)). Supplementary Fig. S1 depicts the locations of air quality monitoring stations and meteorological stations.

2.5. Statistical analysis

To evaluate the performance of the model, hourly WRF-CMAQ output data were interpolated to the observation sites (Supplementary Fig. S1). The model performance was measured using statistical indicators such as Pearson correlation coefficient (R), mean bias (MB), normalized mean bias (NMB), the normalized mean error (NME), the mean fractional bias (MFB), and the mean fractional error (MFE). The calculation function is as follows:

$$R = \frac{\sum_{i=1}^n (M_i - \bar{M}_i)(O_i - \bar{O}_i)}{\sqrt{\sum_{i=1}^n (M_i - \bar{M}_i)^2} \sqrt{\sum_{i=1}^n (O_i - \bar{O}_i)^2}} \quad (1)$$

$$MB = \frac{1}{n} \sum_{i=1}^n (M_i - O_i) \quad (2)$$

$$NMB = \frac{\sum_{i=1}^n (M_i - O_i)}{\sum_{i=1}^n O_i} \quad (3)$$

$$NME = \frac{\sum_{i=1}^n |M_i - O_i|}{\sum_{i=1}^n O_i} \quad (4)$$

$$MFB = \frac{1}{n} \sum_{i=1}^n \frac{(M_i - O_i)}{(O_i + M_i/2)} \quad (5)$$

$$MFE = \frac{1}{n} \sum_{i=1}^n \frac{|M_i - O_i|}{(O_i + M_i/2)} \quad (6)$$

Where M_i and O_i are the simulated and observed values of time i , and n is the number of samples. According to the criteria proposed by Boylan and Russell (2006) for the evaluation of chemical transport models, when $-60\% \leq MFB \leq 60\%$, and $MFE \leq 75\%$, the simulation results of the model are considered to be within an acceptable range. If $-30\% \leq MFB \leq 30\%$, and $MFE \leq 50\%$, then the model simulation results are considered excellent and within the ideal range.

In this study, the performance of the WRF model was evaluated using 2 m temperature (T2), 10 m wind speed (WS10), and the performance of

the CMAQ model was evaluated using hourly PM_{2.5} concentrations.

3. Model evaluation

3.1. Meteorological condition

The WRF model performance was evaluated by comparing simulation results of the LULC2017 case with ground observation data, as shown in Supplementary Table 1. The WRF model reproduced the diurnal pattern of T2 with R values ranging from 0.83 to 0.86, and the simulation performance in July was better than that in January, with an MB of 0.04 °C, and NMB and NME of -0.16% and 8.03%, respectively. For WS10, while WRF tended to overestimate wind speed, the simulated wind fields were generally consistent with observations. The R values were 0.70 (January) and 0.55 (July). The lower NMB (11.47% in January and 14.55% in July) indicates that the WRF model has a relatively good simulation performance for WS10. The time series of simulated and observed values for T2 and WS10 at the LJ station is shown in Supplementary Fig. S2 and Supplementary Fig. S3, respectively. The missing data for these observations was <5%; hence, WRF can capture the time variation and magnitude of T2 and WS10 reliably.

3.2. PM_{2.5} concentrations

The CMAQ model performance was evaluated by comparing simulation hourly PM_{2.5} concentrations of the LULC2017 case with ground observation data, as shown in Supplementary Table 2. FPF and SWZ were selected as the city and the background monitoring stations, respectively, for which <5% of the missing data were available. In January, R was 0.61 and 0.56 at FPF and SWZ, respectively; the MFB and MFE met the excellent criteria at FPF (3.46% and 38.65%, respectively), but were in the acceptable range at SWZ (-59.23% and 60.84%, respectively). In July, the CMAQ tended to overestimate PM_{2.5} concentrations, but was able to simulate the daily trend of PM_{2.5}, with MFB (18.61% at FPF, 6.96% at SWZ) and MFE (39.16% at FPF, 37.31% at SWZ) both reaching the excellent standard. As shown in Supplementary Fig. S4 and Supplementary Fig. S5, the WRF-CMAQ was able to capture significant pollution processes during most of the simulation periods and agreed with the variability of the observed values. The deviation may be related to the uncertainty of the parameter scheme and emission inventory. Overall, the WRF-CMAQ model performed well, and the simulated data could be used for further analysis and discussion.

4. Results and discussion

4.1. Impact of land use change on meteorology

LULC changes can alter surface properties, such as thermal inertia, surface albedo, and surface roughness, affecting the surface energy balance and thus affecting the boundary layer meteorology and air quality (Li et al., 2019).

4.1.1. Surface energy budget

Fig. 3 presents the spatial changes of the sensible heat flux caused by LULC alteration via urbanization in Changchun (LULU2017 minus LULC2001, representing the effect of urbanization) in January and July. It is clear that the sensible heat fluxes in the urban expansion area (i.e., area where croplands converted to urban surface from 2001 to 2017, UEA) generally show an increasing trend, reaching a maximum value of 154 W/m² in January and 162 W/m² in July (Supplementary Fig. S6). This is due to the fact that the higher heat capacity of the artificial material makes the urban surface absorb more solar radiation and store more heat, resulting in a significant increase in the sensible heat flux. Fig. 4 presents the spatial changes of the latent heat flux caused by LULC alteration in Changchun in January and July. It can be seen that the latent heat flux of UEA decreases significantly during the daytime, by

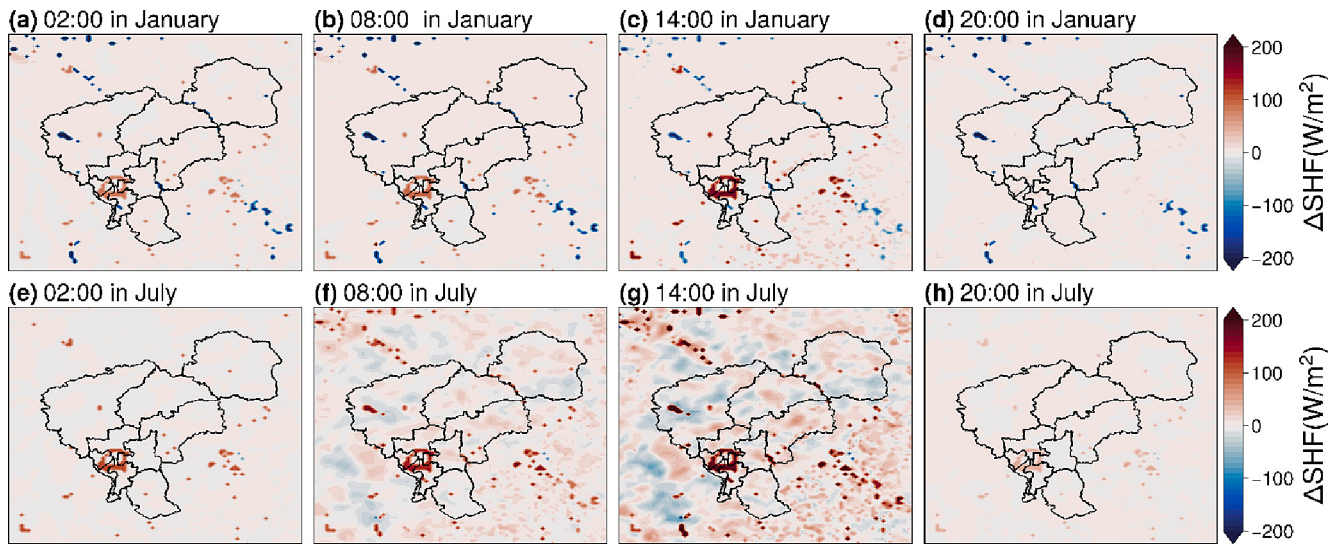


Fig. 3. Spatial patterns of sensible heat flux variations (SHF) induced by land use change between LULC2017 and LULC2001 at 02:00, 08:00, 14:00, and 20:00 in January ((a)-(c)) and July ((d)-(f)).

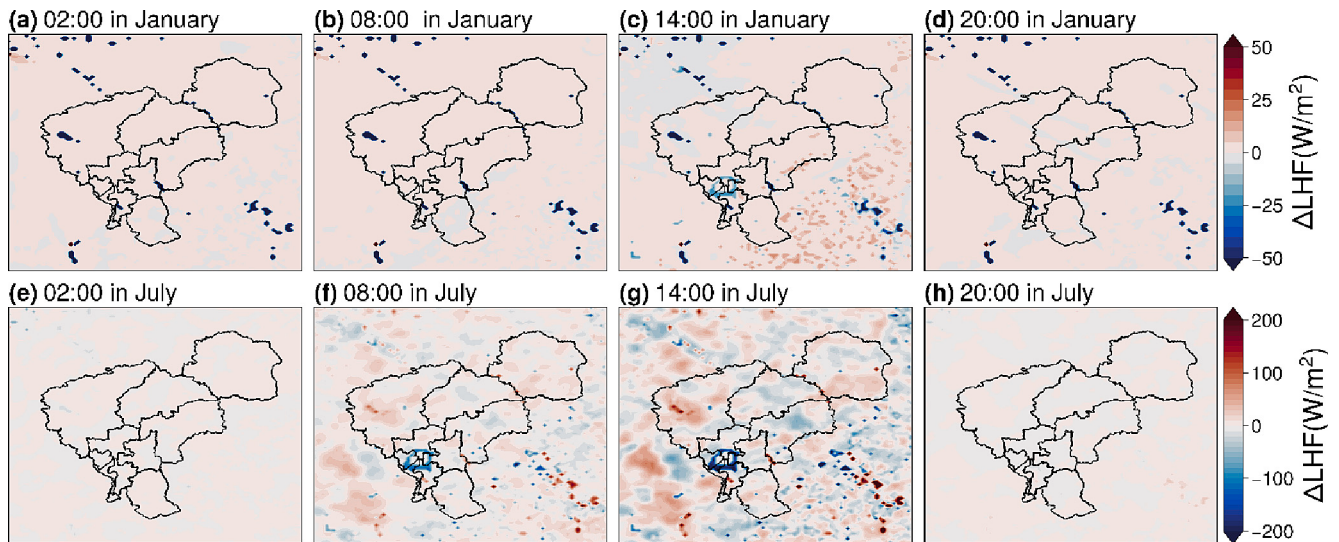


Fig. 4. Spatial patterns of latent heat flux variations (LHF) induced by land use change between LULC2017 and LULC2001 at 02:00, 08:00, 14:00, and 20:00 in January ((a)-(c)) and July ((d)-(f)).

22.84 W/m² in January and 180.75 W/m² in July (Supplementary Fig. S7). This can be attributed to the increase in impermeable surfaces such as cement roads and the decrease in green vegetation coverage when the land use type is changed from croplands to urban land use, resulting in weaker urban evapotranspiration and therefore a significant decrease in latent heat flux in the UEA.

4.1.2. 2 m temperature

Fig. 5 presents the spatial changes of T2 caused by LULC alteration via urbanization across Changchun (LULC2017 minus LULC2001, representing the effect of urbanization) in January and July. Notably, the most significant warming occurred in the UEA, with slight warming in the suburbs and surrounding areas of UEA.

At night, UEA experienced significant warming with a maximum of 4 °C in January and 3 °C in July. In contrast, during the daytime, the warming trend slows down, with T2 changes <1 °C in January and 0.5 °C in July. This pattern is mainly caused by the transformation of croplands to urban land use. The emergence of manmade materials such as cement roads and buildings has led to an increase in thermal capacity

and thermal inertia in urban areas, as well as a decrease in surface albedo. At night, as more solar short-wave radiation is absorbed by urban canopy during the day, the sensible heat flux in urban areas increases, resulting in more energy being released at night and a significant increase in surface temperature. During the daytime, the decrease of vegetation and the increase of impermeable surfaces in urban areas lead to a decrease in urban evapotranspiration, in turn resulting in a decrease in latent heat flux, while the increase of T2 in the UEA is relatively slight, which could be attributed to the higher thermal inertia of the urban canopy hinders the warming process during the day.

In addition, a seasonal change is found with larger increase of T2 in January than that in July. This phenomenon may attributable to the impact of urban interiors on the energy balance, namely, the shadow effects (SE) of urban buildings (street canyons appears in the shaded areas of buildings, resulting in a reduction in solar short-wave radiation reaching the ground)(Liao et al., 2014). In January, lower solar elevation angles result in less solar radiation reaching the ground, which subsequently leads to less radiation being shaded by urban buildings. In July, higher solar elevation angles result in more solar radiation

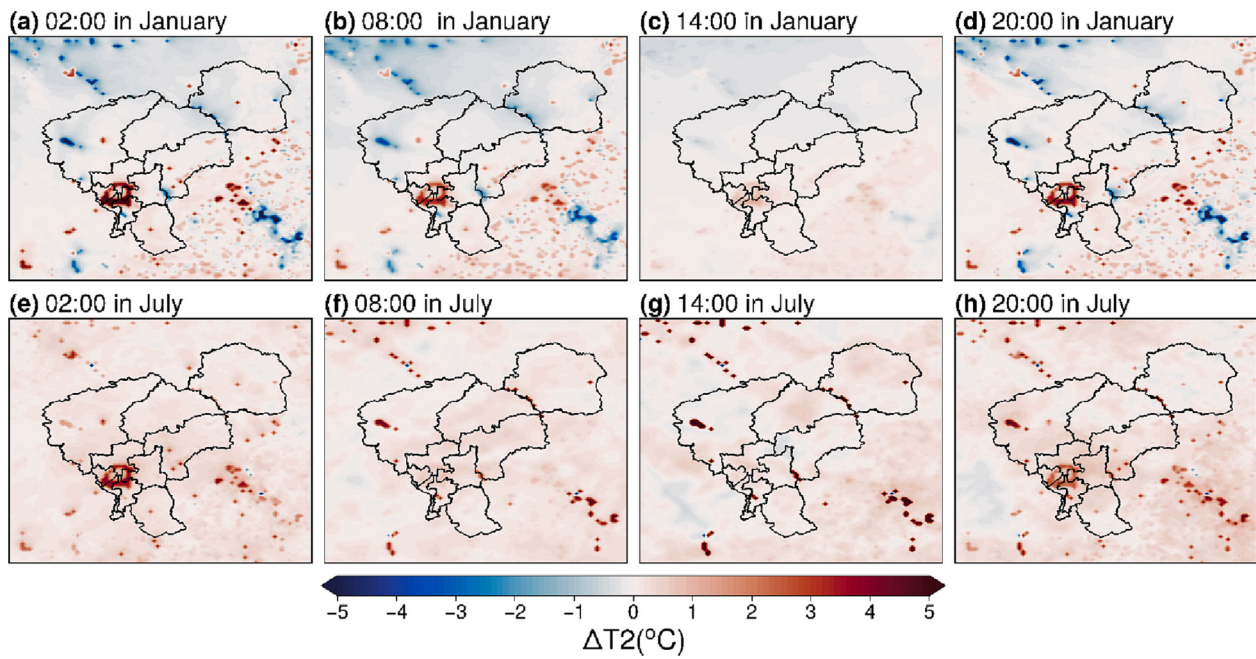


Fig. 5. Spatial patterns of 2 m temperature (T2) variations induced by land use change between LULC2017 and LULC2001 at 02:00, 08:00, 14:00, and 20:00 in January ((a)-(c)) and July ((d)-(f)).

reaching the ground, which subsequently leads to more radiation being shaded by urban buildings. With a greater SE in July, the temperature difference between the urban surface and croplands surface is insignificant, resulting in a temperature rise of only about 0.5 °C in the UEA.

It should also be noticed that T2 changed significantly in areas with shrinking waters in Changchun and surrounding regions, the larger specific heat capacity of water bodies leads to cooling in winter and warming in summer more slowly than the surrounding area. After the shrinking of the waters, the T2 decreases in January while it increases in July.

4.1.3. 10 m wind speed

Fig. 6 presents the spatial changes of WS10 caused by LULC alteration via urbanization across Changchun in January and July. Similarly, the most prominent changes have occurred in the UEA, with an average increase of 1.05 m/s in January, reaching a maximum value of 1.60 m/s, and an average increase of 1.35 m/s in July, reaching a maximum value of 2.55 m/s.

In January, WS10 in the UEA increased throughout the day, which was mainly attributed to the higher energy difference resulting from the higher temperature difference with the surroundings due to the greater thermal capacity of manmade materials in the UEA. This is similar to the conclusion reached by (Chang et al., 2022) that urbanization has led to

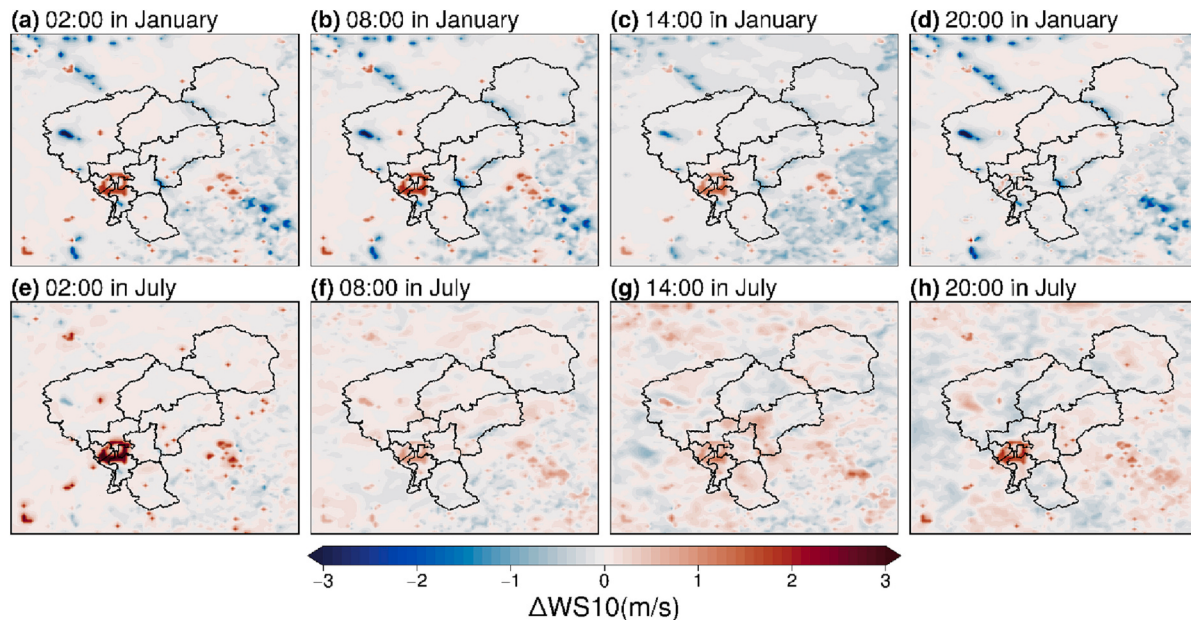


Fig. 6. Spatial patterns of 10 m wind speed (WS10) variations induced by land use change between LULC2017 and LULC2001 at 02:00, 08:00, 14:00, and 20:00 in January ((a)-(c)) and July ((d)-(f)).

an increase in wind speed of 0.5 m/s during the daytime and 1.2 m/s during the nighttime in southern Taiwan, which can be attributed to the heating differences indicated by the urban surface and surrounding croplands. In addition, increasing T2 also enhances the vertical circulation, leading to an increase in surface winds.

In July, the change of WS10 caused by LULC alteration was also similar to that of T2, with a significant increase during the nighttime and a smaller increase during the daytime in the UEA. This phenomenon could be attributed to that manmade materials absorb more solar radiation during the daytime and release more heat during the nighttime. Simultaneously, long-wave radiation in urban street valley is repeatedly reflected and absorbed, delaying the nighttime heat dissipation process, leading to an increase in urban surface temperature and enhancing the aerodynamic energy of atmospheric turbulence. Therefore, WS10 in the UEA significantly increases during the nighttime. During the daytime, the larger SE leads to a less pronounced temperature difference between the urban surface and the surrounding surface, and thus the smaller variation in atmospheric turbulence leads to a weaker effect on the WS10 rise, which rises by about 0.75 m/s over the UEA.

4.1.4. Planetary boundary layer height

Fig. 7 presents the spatial changes of planetary boundary layer height (PBLH) caused by LULC alteration via urbanization across Changchun in January and July. Planetary boundary layer (PBL) is small-scale turbulence caused by wind shear and thermal convection, as part of the near-surface atmosphere near the surface. The PBL affects the mixing and exchange of surface water vapor, heat and upper-level momentum, which is a critical parameter in simulating turbulent mixing, vertical diffusion, convective transport, and deposition of contaminants near the surface (Jia and Zhang, 2021).

In January, the PBLH in the UEA significantly increase during the daytime (10:00–15:00 LST), with a maximum value of 130 m. This is attributed to the increased T2 and sensible heat flux. After sunrise (approximately 05:00 LST), solar radiation begins to heat the air on the ground and the temperature gradually increases, promoting atmospheric turbulence activity, and considering the higher thermal capacity of the urban canopy, the PBL grows faster in LULC2017 scenario than that in LULC2001 scenario due to increased vertical mixing, resulting in differences in PBLH. The greater increase in sensible heat flux during the daytime results in a more pronounced increase in PBLH during the

daytime, while a weaker increase during the nighttime. In contrast, stronger solar radiation in summer leads to more unstable atmosphere, and subsequently resulting in an increase in PBLH, and thus the PBLH increases by 117 m on average in July over the UEA, reaching a maximum value of 420 m.

4.2. Effects of land use change on PM_{2.5}

As previously discussed, LULC changes can affect temperature, wind speed, and other meteorological conditions. These changes will further affect air quality by influencing the formation of air pollutants as well as horizontal transport and vertical dispersion (Fang et al., 2022). As PM_{2.5} is the main pollutant in Changchun City, this section takes PM_{2.5} as an example and focuses on the impact of meteorological changes caused by LULC changes on the temporal and spatial distribution of PM_{2.5} concentrations.

4.2.1. Spatial patterns of PM_{2.5} concentration changes

Fig. 8 presents the spatial changes of PM_{2.5} concentrations caused by LULC alteration across Changchun in January and July. In January, the PM_{2.5} concentrations significantly decreased throughout the day in the UEA, with a maximum of approximately 34 µg/m³, while the PM_{2.5} concentrations increased with a range of 10–30 µg/m³ in the surrounding areas of UEA. In July, the PM_{2.5} concentrations decreased by approximately 20 µg/m³ during the nighttime in the UEA, while the change was not significant during the daytime. This is mainly related to the increase in WS10 and PBLH of the UEA. In January, increased WS10 of UEA promotes the horizontal diffusion of PM_{2.5}, leading to decrease of PM_{2.5} concentrations in the UEA, while PM_{2.5} concentrations increase in the surrounding areas of UEA due to the transport of aerosol particles. In July, the elevated T2 of UEA caused the near surface atmosphere to be warmer than the surrounding areas. The rising branches of the urban heat island circulation enhanced the urban turbulent mixing and upward transport, promoting the development of the planetary boundary layer. More aerosol particles in urban areas were brought to the upper atmosphere and diluted in the boundary layer, thereby reducing the surface PM_{2.5} concentrations in urban areas. In addition, the gas-particle phase partitioning is beneficial for the gas phase of some semi-volatile compounds (i.e. nitrate aerosols and some SOA species) (Li et al., 2019) in PM_{2.5} due to the increased T2 of UEA, resulting in lower PM_{2.5}

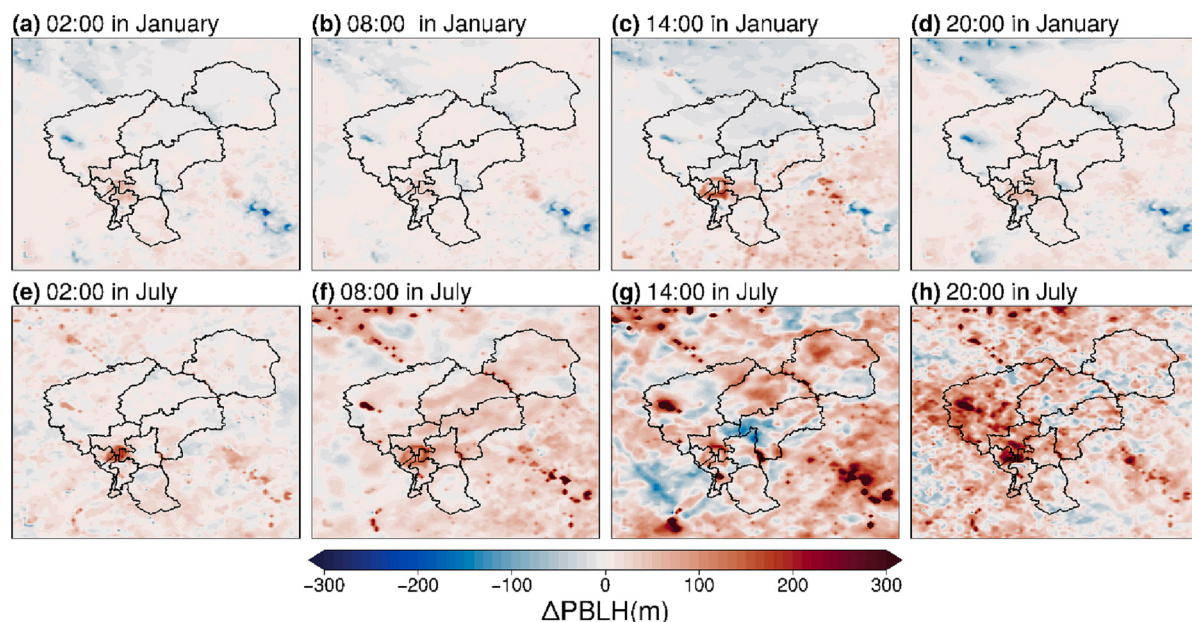


Fig. 7. Spatial patterns of planetary boundary layer height (PBLH) variations induced by land use change between LULC2017 and LULC2001 at 02:00, 08:00, 14:00, and 20:00 in January ((a)-(c)) and July ((d)-(f)).

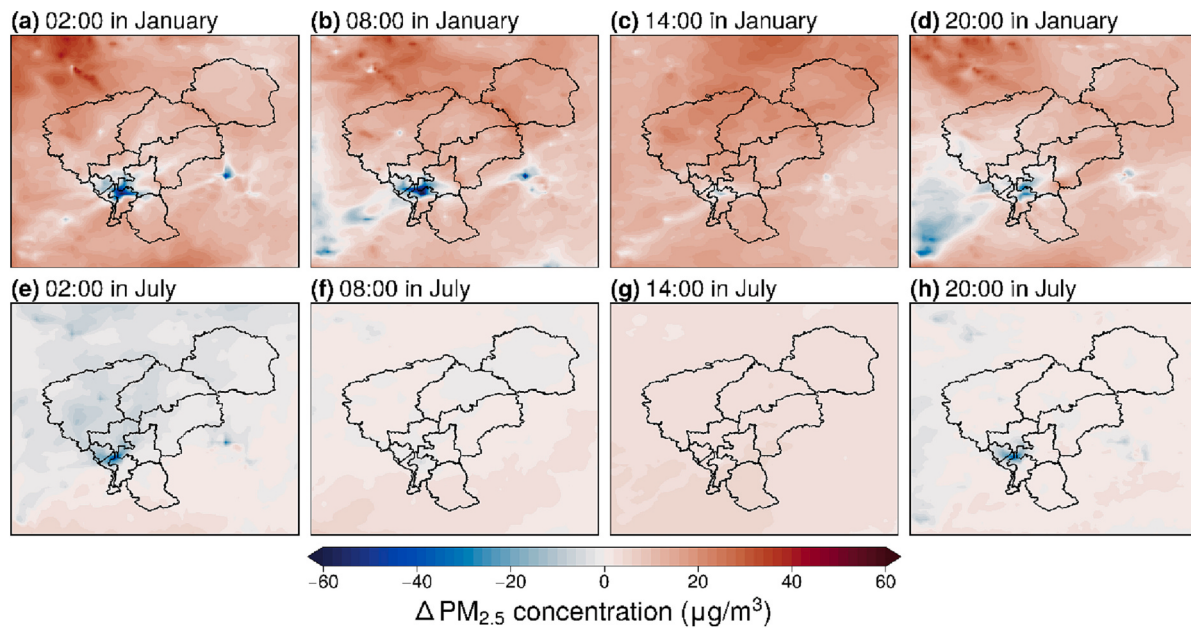


Fig. 8. Spatial patterns of PM_{2.5} concentrations variation induced by land use change between LULC2017 and LULC2001 at 02:00, 08:00, 14:00, and 20:00 in January ((a)-(c)) and July ((d)-(f)).

concentrations of UEA. The change in PM_{2.5} concentrations reflects two key modes of PM_{2.5} diffusion. Horizontal diffusion mainly depends on the increase of surface wind speed, while vertical diffusion requires a higher urban boundary layer, which is related to temperature (Xu and Chen, 2021).

4.2.2. Diurnal patterns of PM_{2.5} and chemical components changes

To further examine the dominant contributor that leads to variations of PM_{2.5}, the chemical components of PM_{2.5} are mainly classified into the following three categories: secondary inorganic aerosols (SNA), including nitrate (NO_3^-), sulfate (SO_4^{2-}), and ammonium (NH_4^+); secondary organic aerosol (SOA), including SOA formed from

anthropogenic VOC precursors (ASOA) and biogenic volatile organic compounds (BVOC) precursors (BSOA); and elemental carbon (EC). In the CMAQ model, PM_{2.5} components could be calculated by combine tool, built for post-processing CMAQ output.

Fig. 9 depicts the diurnal changes of PM_{2.5} components and total PM_{2.5} concentrations across the UEA in January. The LULC change leads to a significant decrease in PM_{2.5} concentrations in the UEA during the nighttime, with a magnitude of approximately 15–35 $\mu\text{g}/\text{m}^3$, and a slight decrease of 2–8 $\mu\text{g}/\text{m}^3$ occurred between 11:00 and 15:00. The change trend of SO_4^{2-} is similar to that of PM_{2.5} concentrations, with a decrease of about 5–6 $\mu\text{g}/\text{m}^3$ during the nighttime, accounting for about 25% of the total concentration change of PM_{2.5}. and a slight decrease of 2–3 $\mu\text{g}/\text{m}^3$

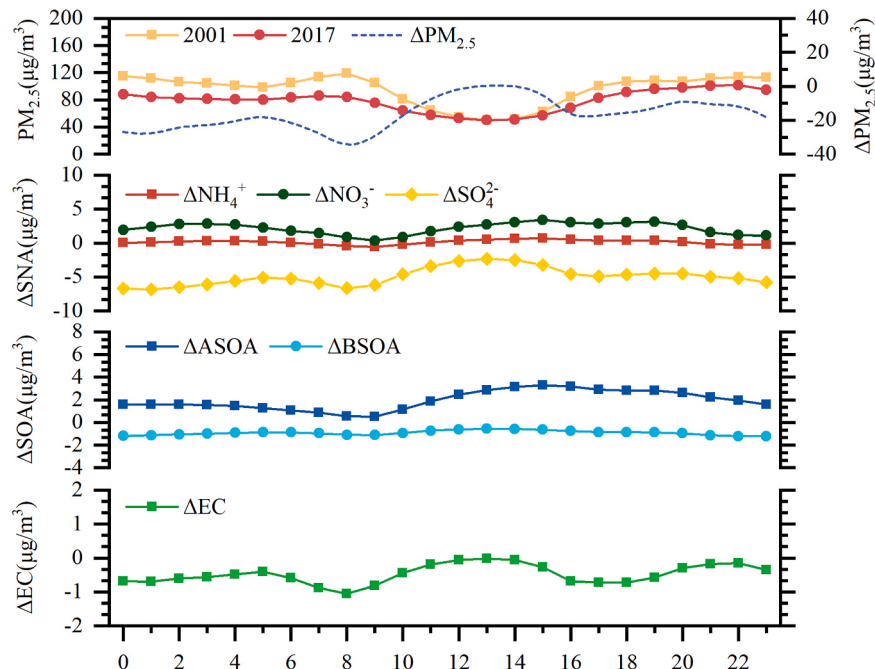


Fig. 9. Diurnal patterns of PM_{2.5} concentrations and chemical components variations induced by land use change between LULC2017 and LULC2001 in January. The average data was calculated from the value of urban expansion area (UEA).

m^3 occurred between 11:00 and 15:00. This pattern can be attributed to the increased surface wind speed accelerating the transmission and diffusion of $\text{PM}_{2.5}$. The concentrations of NO_3^- increased slightly by about $2 \mu\text{g}/\text{m}^3$. This is due to that NO_3^- is semi-volatile and elevated temperature accelerates the gas and liquid phase chemical reaction rates. Compared to SO_4^{2-} and NO_3^- , there is almost no change in NH_4^+ , which is due to the relatively small proportion of NH_3 emissions in CMAQ simulation, and therefore the small change in NH_4^+ in $\text{PM}_{2.5}$. The change trend of ASOA is also similar to that of $\text{PM}_{2.5}$ concentrations, with some semi-volatile substances slightly increasing, with a maximum increase of $3.3 \mu\text{g}/\text{m}^3$ at 15:00. After the conversion of vegetable-based croplands to urban land use, the vegetation leaf area decreased, and subsequently led to a decrease in the isoprene (ISOP) in the UEA (Supplementary Fig. S8), one of the main components of BVOCs, resulting in BSOA concentrations in the UEA decreased by $1 \mu\text{g}/\text{m}^3$ in January. The variation of EC induced by LULC changes decreased with increasing WS10, which is due to the chemical stability of EC, and EC is generally used as a tracer of anthropogenic primary source emissions.

Fig. 10 depicts the diurnal changes of $\text{PM}_{2.5}$ components and total $\text{PM}_{2.5}$ concentrations across the UEA in July. The change trends for $\text{PM}_{2.5}$ concentrations and SO_4^{2-} in the UEA were similar, decreasing by $13\text{--}23 \mu\text{g}/\text{m}^3$ and $1\text{--}3 \mu\text{g}/\text{m}^3$ during the nighttime, respectively, and little change during the daytime. Compared to January, there was almost no change in NO_3^- concentrations in July, which may be due to that the temperature increase in July was not as large as in January, and thus there are lighter impact on the rate of NO_3^- production. Moreover, the lower $\text{PM}_{2.5}$ concentrations level in July results in an insignificant change in NO_3^- concentrations. ASOA concentrations increase slightly from 08:00–23:00, with a maximum increase of about $2 \mu\text{g}/\text{m}^3$ (12:00). Due to the higher emissions of biogenic VOC (BVOC) in summer, the variation of BSOA is greater, with a decrease of approximately $2 \mu\text{g}/\text{m}^3$ during the nighttime. The change trend of EC in July is similar to that in January, with a slight decrease approximately $1 \mu\text{g}/\text{m}^3$ during the nighttime.

4.2.3. Diurnal patterns of physical and chemical processes changes for $\text{PM}_{2.5}$

Fig. 11 depicts the diurnal changes in the contribution of physical

and chemical processes to $\text{PM}_{2.5}$ across the UEA in January under LULC2001 and LULC2017. CHEM and HDIF processes were insignificantly affected by LULC changes, while AERO process remarkable decrease by $4\text{--}6 \mu\text{g}/\text{m}^3$ between 08:00–12:00. This could be attributed to the lower T2 under LULC2001 are more conducive to the formation and stability of secondary aerosols. DDEP process enhanced and increased the negative contribution to $\text{PM}_{2.5}$ concentrations. Compared to the LULC2001 scenario, the amount of $\text{PM}_{2.5}$ concentrations reduction caused by DDEP under the LULC2017 scenario has nearly doubled, with a maximum value of $3.05 \mu\text{g}/\text{m}^3$ (10:00 LST). The ZADV process is significantly enhanced during the daytime, with an increase in the negative contribution to $\text{PM}_{2.5}$ of $25 \mu\text{g}/\text{m}^3$ (12:00 LST). The enhanced VDIF process resulted in an increase in the magnitude of $\text{PM}_{2.5}$ concentration reduction by $20 \mu\text{g}/\text{m}^3$ during the daytime and $40 \mu\text{g}/\text{m}^3$ during the nighttime, respectively. This could be attributed to the increasing kinetic energy of the atmospheric turbulence due to the significant increased T2 induced by LULC changes, enhancing the vertical diffusion. The negative contribution of the HADV process to $\text{PM}_{2.5}$ increased by $40 \mu\text{g}/\text{m}^3$, and this difference may be due to the increase in surface wind speed that intensifies the horizontal movement of the atmosphere. The main reason for the decrease in $\text{PM}_{2.5}$ concentrations across the UEA in January due to the LULC changes is attributable to the enhancement of transport and diffusion in the horizontal and vertical directions.

Fig. 12 depicts the diurnal changes in the contribution of physical and chemical processes to $\text{PM}_{2.5}$ across the UEA in July under LULC2001 and LULC2017. The effect of LULC variation on CHEM, HDIF, DDEP, and ZADV processes is not significant. Due to the lower $\text{PM}_{2.5}$ concentrations in July, the magnitude of change in the AERO process was slightly less than in January, with a reduction of $2\text{--}4 \mu\text{g}/\text{m}^3$. The VDIF and HADV processes are significantly enhanced during the nighttime, with the maximum increase in negative contributions to $\text{PM}_{2.5}$ reaching $40 \mu\text{g}/\text{m}^3$ and $32 \mu\text{g}/\text{m}^3$, respectively. The decrease in $\text{PM}_{2.5}$ concentrations in Changchun in July is due to the LULC changes is also the enhancement of transport and diffusion in the horizontal and vertical directions.

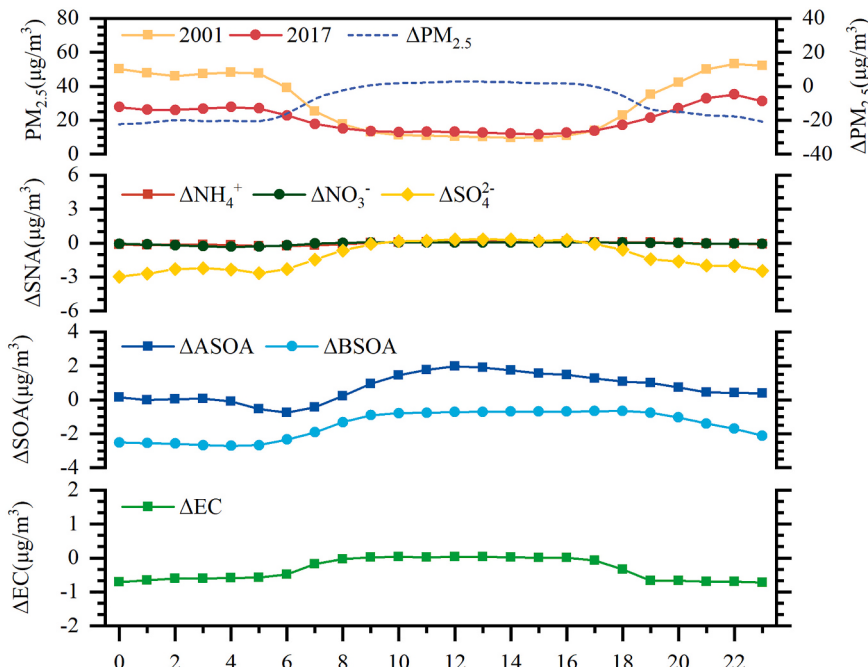


Fig. 10. Diurnal patterns of $\text{PM}_{2.5}$ concentrations and chemical components variations induced by land use change between LULC2017 and LULC2001 in July. The average data was calculated from the value of urban expansion area (UEA).

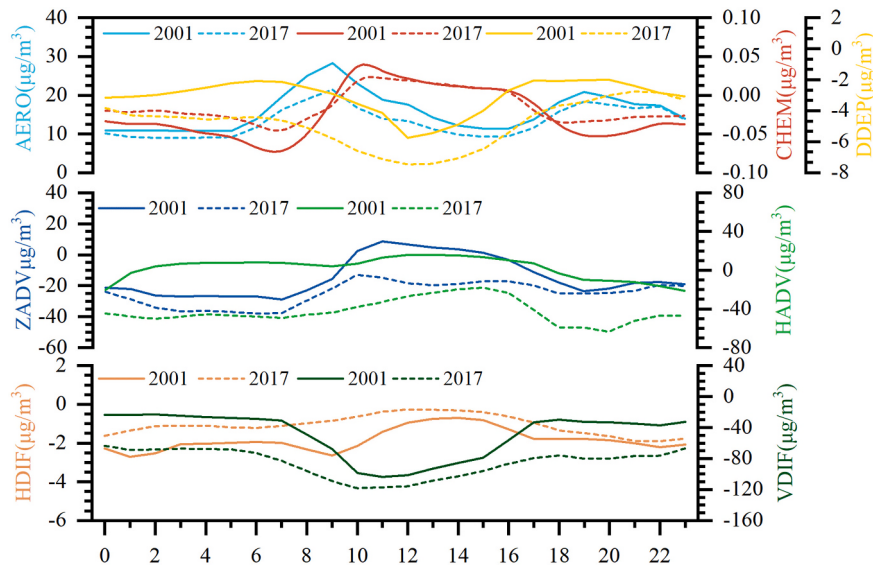


Fig. 11. Diurnal patterns of physical and chemical processes for $\text{PM}_{2.5}$ in LULC2017 and LULC2001 in January. The average data was calculated from the value of urban expansion area (UEA).

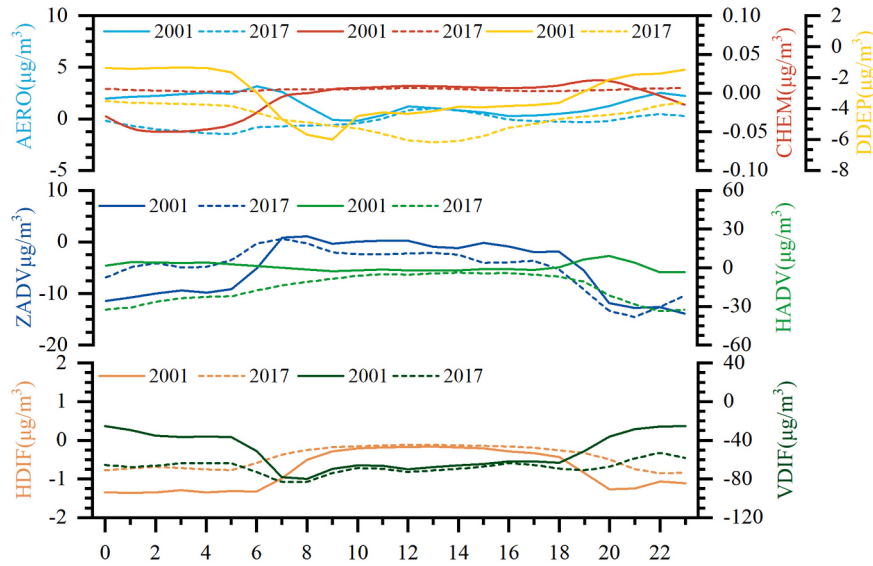


Fig. 12. Diurnal patterns of physical and chemical processes for $\text{PM}_{2.5}$ in LULC2017 and LULC2001 in July. The average data was calculated from the value of urban expansion area (UEA).

5. Conclusions

We used WRF-CMAQ to simulate LULC2017 (based on LULC data from MODIS2017) and LULC2001 (based on LULC data from MODIS2001) scenarios to investigate the effects of LULC changes on meteorology and $\text{PM}_{2.5}$ concentrations in Changchun. Except for LULC data, all physical and chemical schemes, as well as anthropogenic emission inventories were identical in both the LULC2017 and LULC2001 scenarios, hence the differences in these two simulation results allow quantification of the impacts of LULC changes on meteorology and $\text{PM}_{2.5}$ concentrations in Changchun. According to model evaluation using the observed data, the WRF-CMAQ model captures the spatial and temporal evolution of meteorological and air pollutants in Changchun accurately.

Our results find that significant meteorological changes have occurred in urban expansion area (i.e., area where croplands converted to urban surface from 2001 to 2017, UEA). T_2 increased by 4°C and 3°C

during the nighttime in January and July, respectively, while the warming trend is relatively slow during the daytime, with 1°C and 0.5°C in January and July, respectively. WS10 increased by 1.05 m/s and 1.60 m/s in January and July, respectively. PBLH increased by 100 m and 117 m in January and July, respectively. The sensible heat flux increased significantly during the daytime, reaching 154 W/m and 162 W/m^2 in January and July, respectively, while the latent heat flux decreased significantly during the daytime, reaching 22.84 W/m^2 and 180.75 W/m^2 in January and July, respectively. Regional meteorological changes further affect chemical evolution and air quality. LULC changes lead to an overall decreasing trend of $\text{PM}_{2.5}$ in the UEA, reaching $34 \text{ } \mu\text{g/m}^3$ and $20 \text{ } \mu\text{g/m}^3$ in January and July, respectively. Similar to the change trend of total $\text{PM}_{2.5}$ concentrations, SO_4^{2-} decreased significantly by about $5\text{--}6 \text{ } \mu\text{g/m}^3$ at night in January, accounting for about 25% of the change in total $\text{PM}_{2.5}$ concentrations. SOA formed from biogenic VOC precursors (BSOA) slightly decreased due to the reduction of the croplands dominated by green vegetation. While,

$\text{PM}_{2.5}$ concentrations in the surrounding areas of the UEA increased significantly in January. The results of the process analysis based on the CMAQ model indicate that the main reason for this spatial variation of $\text{PM}_{2.5}$ concentrations is the enhancement of transport and diffusion in the horizontal and vertical directions in the UEA. In January, the negative contribution of ZADV and HADV processes to $\text{PM}_{2.5}$ in the UEA increased by 25 $\mu\text{g}/\text{m}^3$ and 40 $\mu\text{g}/\text{m}^3$, respectively. VDIF process caused an increase in $\text{PM}_{2.5}$ diffusion by 40 $\mu\text{g}/\text{m}^3$ and 16 $\mu\text{g}/\text{m}^3$ during the daytime and nighttime in the UEA, respectively. In July, the negative contribution of VDIF and HADV processes to $\text{PM}_{2.5}$ increased by 40 $\mu\text{g}/\text{m}^3$ and 32 $\mu\text{g}/\text{m}^3$ during the nighttime in the UEA, respectively. This indicates that the enhancement of transport and diffusion in the horizontal and vertical directions in the UEA maybe beneficial to the decrease of $\text{PM}_{2.5}$ concentrations in the UEA and the increase of $\text{PM}_{2.5}$ concentrations in the surrounding areas of the UEA.

This study has quantified the effects of urbanization on meteorology and air quality in Changchun, an old industrial base city in Northeast China, with significant implications for the development of effective regional air management policies and sustainable development strategies. In future urban construction, it is worthwhile for government departments to consider increasing the area of urban green vegetation coverage and surface albedo, as well as the planning of scattered small and medium-sized cities. In addition to the direct effects of LULC changes, changes in pollutant emissions and anthropogenic heat fluxes due to urban expansion can have significant impacts on meteorology and air quality in urban areas, and these issues should be addressed and compared in the future.

Financial support

This work was supported by the Ecology and Environment Department of Jilin Province (2018-19 and 2019-08).

CRediT authorship contribution statement

Jiaxin Qiu: Conceptualization, Methodology, Formal analysis, Investigation, Writing – original draft, Visualization. **Chunsheng Fang:** Conceptualization, Writing – review & editing, Project administration. **Naixu Tian:** Conceptualization, Visualization. **Haofan Wang:** Conceptualization, Visualization. **Ju Wang:** Conceptualization, Project administration.

Declaration of Competing Interest

The authors declare that they have no conflict of interest.

Data availability

The NCEP FNL dataset can be freely downloaded from <https://rda.ucar.edu/datasets/ds083.2/>. The anthropogenic emissions are provided by the MEIC team (<http://www.meicmodel.org/>).

Acknowledgements

The authors would like to thank the group members of Laboratory 537 and 142 of Jilin University for their help and guidance for this study. Additionally, the authors would like to thank the MEIC team from Tsinghua University for providing the Multiscale Emission Inventory of China (MEIC).

Appendix A. Supplementary data

Supplementary data to this article can be found online at <https://doi.org/10.1016/j.atmosres.2023.106759>.

References

- Boylan, J.W., Russell, A.G., 2006. PM and light extinction model performance metrics, goals, and criteria for three-dimensional air quality models. *Atmos. Environ.* 40, 4946–4959. <https://doi.org/10.1016/j.atmosenv.2005.09.087>.
- Chen, S.-H., Sun, W.-Y., 2002. A one-dimensional time dependent cloud model. *J. Meteorol. Soc. Jpn.* 80 (1), 99–118. <https://doi.org/10.2151/jmsj.80.99>.
- Chen, Z., Zhang, Y., 2022. Quantitative Identification of Temporal-Spatial Variations of Urban Heat Island (UHI) Effects in Changchun, China. *IEEE J.Select.Top.Appl.Earth Observ.Remote Sens.* 15, 3052–3060. <https://doi.org/10.1109/JSTARS.2022.3167831>.
- Chen, B., Yang, S., Xu, X.-D., Zhang, W., 2014. The impacts of urbanization on air quality over the Pearl River Delta in winter: roles of urban land use and emission distribution. *Theor. Appl. Climatol.* 117, 29–39. <https://doi.org/10.1007/s00704-013-0982-1>.
- Chen, X., Gu, X., Zhan, Y., Wang, D., Zhang, Y., Mumtaz, F., Shi, S., Liu, Q., 2022. The impact of central heating on the urban thermal environment based on multi-temporal remote sensing images. *Remote Sens.* 14, 2327. <https://doi.org/10.3390/rs14102327>.
- Chou, M.-D., Suarez, M.J., Liang, X.-Z., Yan, M.M.-H., Cote, C., 2001. A Thermal Infrared Radiation Parameterization for Atmospheric Studies.
- Civerolo, K., Hogrefe, C., Lynn, B., Rosenthal, J., Ku, J.-Y., Solecki, W., Cox, J., Small, C., Rosenzweig, C., Goldberg, R., Knowlton, K., Kinney, P., 2007. Estimating the effects of increased urbanization on surface meteorology and ozone concentrations in the New York City metropolitan region. *Atmos. Environ.* 41, 1803–1818. <https://doi.org/10.1016/j.atmosenv.2006.10.076>.
- Dong, Y., Ren, Z., Fu, Y., Miao, Z., Yang, R., Sun, Y., He, X., 2020. Recording Urban Land Dynamic and its Effects during 2000–2019 at 15-m Resolution by Cloud Computing with Landsat Series. *Remote Sens.* 12, 2451. <https://doi.org/10.3390/rs12152451>.
- Ek, M.B., Mitchell, K.E., Lin, Y., Rogers, E., Grunmann, P., Koren, V., Gayno, G., Tarpley, J.D., 2003. Implementation of Noah land surface model advances in the National Centers for Environmental Prediction operational mesoscale Eta model. *J. Geophys. Res.-Atmos.* 108. <https://doi.org/10.1029/2002JD003296>.
- Fan, J., Ju, T., Wang, Q., Gao, H., Huang, R., Duan, J., 2021. Spatiotemporal variations and potential sources of tropospheric formaldehyde over eastern China based on OMI satellite data. *Atmos. Pollution Res.* 12, 272–285. <https://doi.org/10.1016/j.apr.2020.09.011>.
- Fang, C., Qiu, J., Li, J., Wang, J., 2022. Analysis of the meteorological impact on $\text{PM}_{2.5}$ pollution in Changchun based on KZ filter and WRF-CMAQ. *Atmos. Environ.* 271, 118924. <https://doi.org/10.1016/j.atmosenv.2021.118924>.
- Guenther, A., Karl, T., Harley, P., Wiedinmyer, C., Palmer, P.I., Geron, C., 2006. Estimates of global terrestrial isoprene emissions using MEGAN (Model of Emissions of gases and Aerosols from Nature). *Atmos. Chem. Phys.* 6, 3181–3210. <https://doi.org/10.5194/acp-6-3181-2006>.
- Huszar, P., Karlický, J., Marková, J., Nováková, T., Liaskoni, M., Bartík, L., 2021. The regional impact of urban emissions on air quality in Europe: the role of the urban canopy effects. *Atmos. Chem. Phys.* 21, 14309–14332. <https://doi.org/10.5194/acp-21-14309-2021>.
- Janjić, Z.I., 1994. The step-mountain eta coordinate model: further developments of the convection, viscous sublayer, and turbulence closure schemes. *Mon. Weather Rev.* 122, 927–945. [https://doi.org/10.1175/1520-0493\(1994\)122<0927:TSMECM>2.0.CO;2](https://doi.org/10.1175/1520-0493(1994)122<0927:TSMECM>2.0.CO;2).
- Jia, W., Zhang, X., 2021. Impact of modified turbulent diffusion of $\text{PM}_{2.5}$ aerosol in WRF-Chem simulations in eastern China. *Atmos. Chem. Phys.* 21, 16827–16841. <https://doi.org/10.5194/acp-21-16827-2021>.
- Kusaka, H., Kimura, F., 2004. Coupling a Single-Layer Urban Canopy Model with a simple Atmospheric Model: Impact on Urban Heat Island simulation for an Idealized Case. *Astro. J.* 82, 67–80. <https://doi.org/10.2151/jmsj.82.67>.
- Li, M., Song, Y., Mao, Z., Liu, M., Huang, X., 2016. Impacts of thermal circulations induced by urbanization on ozone formation in the Pearl River Delta region, China. *Atmos. Environ.* 127, 382–392. <https://doi.org/10.1016/j.atmosenv.2015.10.075>.
- Li, M., Liu, H., Geng, G., Hong, C., Liu, F., Song, Y., Tong, D., Zheng, B., Cui, H., Man, H., Zhang, Q., He, K., 2017. Anthropogenic emission inventories in China: a review. *Natl. Sci. Rev.* 4, 834–866. <https://doi.org/10.1093/nsr/nwx150>.
- Li, Y., Zhang, J., Sailor, D.J., Ban-Weiss, G.A., 2019. Effects of urbanization on regional meteorology and air quality in Southern California. *Atmos. Chem. Phys.* 19, 4439–4457. <https://doi.org/10.5194/acp-19-4439-2019>.
- Liao, J., Wang, T., Wang, X., Xie, M., Jiang, Z., Huang, X., Zhu, J., 2014. Impacts of different urban canopy schemes in WRF/Chem on regional climate and air quality in Yangtze River Delta, China. *Atmos. Res.* 145–146, 226–243. <https://doi.org/10.1016/j.atmosres.2014.04.005>.
- Lu, Y., Yang, X., Wang, H., Jiang, M., Wen, X., Zhang, X., Meng, L., 2023. Exploring the effects of land use and land cover changes on meteorology and air quality over Sichuan Basin, southwestern China. *Front. Ecol. Evol.* 11, 1131389. <https://doi.org/10.3389/fevo.2023.1131389>.
- Ma, R., Ban, J., Wang, Q., Zhang, Y., Yang, Y., He, M.Z., Li, S., Shi, W., Li, T., 2021. Random forest model based fine scale spatiotemporal O₃ trends in the Beijing-Tianjin-Hebei region in China, 2010 to 2017. *Environ. Pollut.* 276, 116635. <https://doi.org/10.1016/j.envpol.2021.116635>.
- Mlawer, E.J., Taubman, S.J., Brown, P.D., Iacono, M.J., Clough, S.A., 1997. Radiative transfer for inhomogeneous atmospheres: RRTM, a validated correlated-k model for the longwave. *J. Geophys. Res.-Atmos.* 102, 16663–16682. <https://doi.org/10.1029/97JD00237>.
- Peng, J., Hu, Y., Dong, J., Liu, Q., Liu, Y., 2020. Quantifying spatial morphology and connectivity of urban heat islands in a megacity: a radius approach. *Sci. Total Environ.* 714, 136792. <https://doi.org/10.1016/j.scitotenv.2020.136792>.

- Shi, G., Lu, X., Zhang, H., Zheng, H., Zhang, Z., Chen, S., Xing, J., Wang, S., 2022. Air pollutant emissions induced by rural-to-urban migration during China's urbanization (2005–2015). *Environ. Sci. Ecotechnol.* 10, 100166 <https://doi.org/10.1016/j.jese.2022.100166>.
- Stoddart, J.C., Dandridge, O., Garner, A., Cobb, J., van Arkel, R.J., 2021. The compartmental distribution of knee osteoarthritis - a systematic review and meta-analysis. *Osteoarthr. Cartil.* 29, 445–455. <https://doi.org/10.1016/j.joca.2020.10.011>.
- Tao, H., Xing, J., Zhou, H., Chang, X., Li, G., Chen, L., Li, J., 2018. Impacts of land use and land cover change on regional meteorology and air quality over the Beijing-Tianjin-Hebei region, China. *Atmos. Environ.* 189, 9–21. <https://doi.org/10.1016/j.atmosenv.2018.06.033>.
- Wang, K., Gao, C., Wang, H., Wu, K., Tong, Q., Dan, M., Ji, X., Tong, Q., 2023. ISAT v2.0: An integrated tool for nested domain configurations and model-ready emission inventories for WRF-AQM. *Geoscientific Model Development Discussions* 1–18. <https://doi.org/10.5194/gmd-16-1961-2023>.
- Wang, X., Liao, J., Zhang, J., Shen, C., Chen, W., Xia, B., Wang, T., 2014. A numeric study of regional climate change induced by urban expansion in the Pearl River Delta, China. *J. Appl. Meteorol. Climatol.* 53, 346–362. <https://doi.org/10.1175/JAMC-D-13-054.1>.
- Wang, H., Liu, Z., Wu, K., Qiu, J., Zhang, Y., Ye, B., He, M., 2022a. Impact of Urbanization on Meteorology and Air Quality in Chengdu, a Basin City of Southwestern China. *Front. Ecol. Evol.* 10, 845801. <https://doi.org/10.3389/fevo.2022.845801>.
- Wang, H., Liu, Z., Zhang, Y., Yu, Z., Chen, C., 2021. Impact of different urban canopy models on air quality simulation in Chengdu, southwestern China. *Atmos. Environ.* 267, 118775 <https://doi.org/10.1016/j.atmosenv.2021.118775>.
- Wang, Y., Yang, X., Wu, K., Mei, H., De Smedt, I., Wang, S., et al., 2022b. Long-term trends of ozone and precursors from 2013 to 2020 in a megacity (Chengdu), China: Evidence of changing emissions and chemistry. *Atmos. Res.* 106309 <https://doi.org/10.1016/j.atmosres.2022.106309>.
- Wei, J., Li, Z., Lyapustin, A., Sun, L., Peng, Y., Xue, W., Su, T., Cribb, M., 2021. Reconstructing 1-km-resolution high-quality PM2.5 data records from 2000 to 2018 in China: spatiotemporal variations and policy implications. *Remote Sens. Environ.* 252 (112136) <https://doi.org/10.1016/j.rse.2020.112136>.
- Wu, K., Wang, Y., Qiao, Y., Liu, Y., Wang, S., Yang, X., et al., 2022a. Drivers of 2013–2020 ozone trends in the Sichuan Basin, China: Impacts of meteorology and precursor emission changes. *Environ. Pollut.* 300, 118914. <https://doi.org/10.1016/j.envpol.2022.118914>.
- Wu, K., Yang, X., Chen, D., Gu, S., Lu, Y., Jiang, Q., et al., 2020. Estimation of biogenic VOC emissions and their corresponding impact on ozone and secondary organic aerosol formation in China. *Atmos. Res.* 231, 104656. <https://doi.org/10.1016/j.atmosres.2019.104656>.
- Wu, X., Zhang, Y., Wang, L., 2022b. Coupling relationship between regional urban development and eco-environment: Inspiration from the old industrial base in Northeast China. *Ecol. Indic.* 142, 109259 <https://doi.org/10.1016/j.ecolind.2022.109259>.
- Xu, H., Chen, H., 2021. Impact of urban morphology on the spatial and temporal distribution of PM2.5 concentration: a numerical simulation with WRF/CMAQ model in Wuhan, China. *J. Environ. Manag.* 290, 112427 <https://doi.org/10.1016/j.jenman.2021.112427>.
- Yang, C., He, X., Yan, F., Yu, L., Bu, K., Yang, J., Chang, L., Zhang, S., 2017. Mapping the influence of land use/land cover changes on the urban heat island effect—a case study of Changchun, China. *Sustainability* 9, 312. <https://doi.org/10.3390/su9020312>.
- Yang, X., Wu, K., Wang, H., Liu, Y., Gu, S., Lu, Y., et al., 2020. Summertime ozone pollution in Sichuan Basin, China: Meteorological conditions, sources and process analysis. *Atmos. Environ.* 226, 117392. <https://doi.org/10.1016/j.atmosenv.2020.117392>.
- Yang, L., Li, X., Shang, B., 2022. Impacts of Urban expansion on the urban thermal environment: a case study of Changchun, China. *Chin. Geogr. Sci.* 32, 79–92. <https://doi.org/10.1007/s11769-021-1251-3>.
- Yang, C., Zhu, W., Sun, J., Xu, X., Wang, R., Lu, Y., Zhang, S., Zhou, W., 2021a. Assessing the effects of 2D/3D urban morphology on the 3D urban thermal environment by using multi-source remote sensing data and UAV measurements: a case study of the snow-climate city of Changchun, China. *J. Clean. Prod.* 321, 128956 <https://doi.org/10.1016/j.jclepro.2021.128956>.
- Yang, X., Wu, K., Lu, Y., Wang, S., Qiao, Y., Zhang, X., et al., 2021b. Origin of regional springtime ozone episodes in the Sichuan Basin, China: role of synoptic forcing and regional transport. *Environ. Pollut.* 116845 <https://doi.org/10.1016/j.envpol.2021.116845>.
- Yu, M., Carmichael, G.R., Zhu, T., Cheng, Y., 2014. Sensitivity of predicted pollutant levels to anthropogenic heat emissions in Beijing. *Atmos. Environ.* 89, 169–178. <https://doi.org/10.1016/j.atmosenv.2014.01.034>.
- Zhang, N., Gao, Z., Wang, X., Chen, Y., 2010. Modeling the impact of urbanization on the local and regional climate in Yangtze River Delta, China. *Theor. Appl. Climatol.* 102, 331–342. <https://doi.org/10.1007/s00704-010-0263-1>.
- Zheng, B., Tong, D., Li, M., Liu, F., Hong, C., Geng, G., Li, H., Li, X., Peng, L., Qi, J., Yan, L., Zhang, Y., Zhao, H., Zheng, Y., He, K., Zhang, Q., 2018. Trends in China's anthropogenic emissions since 2010 as the consequence of clean air actions. *Atmos. Chem. Phys.* 18, 14095–14111. <https://doi.org/10.5194/acp-18-14095-2018>.
- Zhu, K., Xie, M., Wang, T., Cai, J., Li, S., Feng, W., 2017. A modeling study on the effect of urban land surface forcing to regional meteorology and air quality over South China. *Atmos. Environ.* 152, 389–404. <https://doi.org/10.1016/j.atmosenv.2016.12.053>.